M. Oschatz, W. Nickel, M. Thommes, K. A. Cychosz, M. Leistner, M. Adam, G. Mondin, P. Strubel, L. Borchardt, S. Kaskel

Evolution of porosity in carbide-derived carbon aerogels

Erstveröffentlichung in / First published in:
Journal of Materials Chemistry A. 2014, 2(43), S. 18472–18479 [Zugriff am: 01.11.2019]. Royal Society of Chemistry. ISSN 2050-7496.

DOI: https://doi.org/10.1039/c4ta03401e

Journal of Materials Chemistry A

PAPER

View Article Online
View Journal | View Issue

Cite this: J. Mater. Chem. A, 2014, 2, 18472

Evolution of porosity in carbide-derived carbon aerogels†

M. Oschatz,[a] W. Nickel,[a] M. Thommes,[b] K. A. Cychosz,[b] M. Leistner,[c] M. Adam,[a] G. Mondin,[a] P. Strubel,[c] L. Borchardt‡[d] and S. Kaskel*[ac]

Received 3rd July 2014
Accepted 4th September 2014

DOI: 10.1039/c4ta03401e

www.rsc.org/MaterialsA

Carbide-derived carbon (CDC) aerogel monoliths with very high porosity are synthesized starting from polymeric precursors. Cross-linking by platinum-catalyzed hydrosilylation of polycarbosilanes followed by supercritical drying yields preceramic aerogels. After ceramic conversion and silicon extraction in hot chlorine gas, hierarchically porous carbon materials with specific surface areas as high as 2122 $m^2\ g^{-1}$ and outstanding total pore volumes close to 9 $cm^3\ g^{-1}$ are obtained. Their pore structure is controllable by the applied synthesis temperature as shown by combined nitrogen (−196 °C) and carbon dioxide (0 °C) measurements coupled with electron microscopic methods. The combination of large micropore volumes and the aerogel-type pore system leads to advanced adsorption properties due to a combination of large storage capacities and effective materials transport in comparison with purely microporous reference materials as shown by thermal response measurements.

Introduction

Carbide-derived carbons (CDCs) are a class of nanoporous carbon materials and have received considerable attention in the last decade.[1] The advanced micropore structure makes CDCs attractive candidates for the use in numerous applications such as gas adsorption and separation,[2] catalysis,[3] protein adsorption,[4] and electrochemical energy storage.[5] These materials are produced by the selective removal of metal- or semi-metal atoms from carbides in an atmosphere of halogens or halogenated compounds leading to the formation of a microporous carbon structure. The transformation from carbide to carbon is fully conformal and the choice of appropriate precursors and halogenation temperatures enable control over the pore size with high accuracy.[6] Therefore, different carbides with various textures (powders,[7] thin films,[8] biomorphic ceramics,[9] and monoliths[10]) can be subjected to this process leading to a large pool of available structures.

By using polymeric precursors instead of bulk carbides, the micropore system of the CDCs can be combined with a secondary pore arrangement leading to the formation of hierarchical structures which combine high specific surface areas with efficient materials transport.[11] Templating approaches[12] are particularly suitable for the formation of mesoporous silicon carbide structures which can be transferred to carbide-derived carbons with combined micro- and transport pores.[13]

Hard templating (also referred to as nanocasting) was applied for the production of ordered mesoporous CDCs (OM-CDCs)[14] and CDC mesofoams[15] with specific surface areas (SSAs) as high as 2900 $m^2\ g^{-1}$ and total pore volumes up to 2.6 $cm^3\ g^{-1}$. In this strategy, the pore systems of mesoporous silica templates are filled with polycarbosilane (PCS) polymers as silicon carbide precursors. After thermal conversion under inert atmosphere and wet chemical template removal in hydrofluoric acid solution, the resulting mesoporous SiC materials can be subjected to high-temperature chlorine treatment and act as precursors for the formation of hierarchical micro-mesoporous CDCs. The choice of appropriate synthesis temperatures, template structures, and infiltration techniques allows for precise control over the microstructure in these materials.[15] OM-CDCs and CDC mesofoams show outstanding performance as electrode materials in electrochemical double-layer capacitors (EDLCs)[15,16] and as the host material for the active component in lithium–sulphur (Li–S) battery cathodes.[15,17]

Alternatively, soft-templating methods[18] can be used to overcome the use of silica templates and their removal with highly toxic chemicals. Polymerized High Internal Phase Emulsions (PolyHIPEs) can be prepared from PCS polymers

[a]Department of Inorganic Chemistry, Dresden University of Technology, Bergstraße 66, D-01062 Dresden, Germany. E-mail: Stefan.Kaskel@chemie.tu-dresden.de

[b]Quantachrome Instruments, 1900 Corporate Drive, Boynton Beach, FL-33426, USA

[c]Fraunhofer Institute for Material and Beam Technology, Winterbergstraße 28, D-01277 Dresden, Germany

[d]Institute for Chemical and Bioengineering, ETH Zürich, Wolfgang-Pauli-Strasse 10, CH-8093 Zürich, Switzerland

† Electronic supplementary information (ESI) available: EDX data, characterization of SiC aerogels, and further adsorption data. See DOI: 10.1039/c4ta03401e

‡ Current address: Department of Inorganic Chemistry, Dresden University of Technology, Bergstraße 66, D-01062 Dresden, Germany

after cross-linking with *para*-Divinylbenzene (*p*-DVB) and transferred to strongly hierarchical CDCs with high macropore volumes and advanced adsorption kinetics.[19] Moreover, evaporation-induced self-assembly (EISA) is a useful approach to produce free-standing films of ordered mesoporous carbide-derived carbons. Tetraethyl orthosilicate or titanium citrate and phenolic resin are used as precursors for the formation of hexagonally ordered silicon or titanium carbide/carbon composites. High-temperature chlorine treatment transforms these materials to CDCs with full retention of the ordered arrangement of mesopores.[13]

Besides microporous carbons, such as CDCs, large-pore carbons such as Kroll-carbons[20] and carbon nanotubes[21] have received considerable attention due to their large and easily accessible pore volumes. Among them, carbon aerogels are of particular interest with regard to their tunable morphology, ultrafine cell sizes, and monolithic appearance.[22] They consist of three-dimensional networks of interconnected nanoparticles, which lead to attractive properties such as low mass densities and high pore volumes. The synthesis of carbon aerogels is carried out by sol–gel techniques that require the conversion of molecular carbon-containing compounds to highly cross-linked gels followed by drying under supercritical conditions and carbonization. Since this procedure does not include the controlled formation of micropores, as-made carbon aerogels show only moderate specific surface areas and micropore volumes. Therefore, post-synthetic activation procedures have to be applied for the insertion of intrinsic nanoporosity. These procedures significantly increase the specific surface area but they are usually accompanied by broadening of the pore size distribution (PSD), formation of irregularly curved pores, and high burn-off.[23]

In this study, we describe the synthesis and structure of hierarchically structured carbide-derived carbon aerogels (designated as DUT-85; DUT: Dresden University of Technology) with ultrahigh porosity. They can be obtained by platinum-catalyzed cross-linking of PCS chains in highly diluted solution using the hydrosilylation reaction[24] followed by supercritical drying, pyrolysis and silicon extraction in hot chlorine gas. DUT-85 materials combine high surface areas and large volumes of narrowly distributed micropores with an aerogel-type pore system leading to extremely high total pore volume and advanced mass transport properties when compared to purely microporous CDCs with similar adsorption capacities. These properties render DUT-85 a highly efficient material for the adsorptive removal of environmentally relevant gases, such as carbon dioxide.[25]

Experimental details

Synthetic procedures

Polycarbosilane aerogels were prepared according to a slightly modified procedure previously reported by Sorarù and co-workers.[24] A mixture of 1.74 g of the allylhydridopolycarbosilane SMP-10 (Starfire Systems) and 1.62 g *para*-divinylbenzene (Sigma Aldrich, 80%) was dissolved in 24.9 g cyclohexane and stirred for 10 min at room temperature (RT). 40 μl of the hydrosilylation catalyzing complex platinum–divinyltetramethyl-disiloxane (Sigma Aldrich, ~2% Pt in xylene) were added and the mixture was stirred for another 5 min at RT followed by hydrothermal treatment in a Teflon-lined autoclave at 200 °C for 1 h. After cooling to RT, the bright yellow gel was transferred to a supercritical drying autoclave and the solvent was exchanged with liquid CO_2 at least twice a day for 5 days. The drying was achieved by raising the temperature of the autoclave to 37 °C and the pressure up to 100–110 bar followed by decreasing the pressure to 1 bar over a period of approximately 2 h. The obtained polycarbosilane aerogels ("PCS aerogel") were pyrolyzed under flowing argon in an alumina tube in a horizontal tubular furnace. Samples were heated to either 700 °C ("SiC aerogel 700 °C") or 1000 °C ("SiC aerogel 1000 °C") at a heating rate of 60 K h^{-1}, maintained at this temperature for 2 h, and cooled down to room temperature under flowing argon. Silicon extraction was performed by high-temperature chlorine treatment by placing approximately 2 g of the SiC aerogel in a quartz boat inside a quartz tube (inner diameter: 25 mm) in a horizontal tubular furnace and heated to the maximum pyrolysis temperature ("DUT-85 700 °C" or "DUT-85 1000 °C") at a rate of 450 K h^{-1} under an argon flow of 150 ml min^{-1}. At the desired temperature the gas flow was changed to a mixture of 80 ml min^{-1} chlorine and 70 ml min^{-1} argon. After 3 h of chlorination the furnace was cooled down to 600 °C under 150 ml min^{-1} argon and maintained for 1 h followed by changing the gas flow to 80 ml min^{-1} hydrogen in order to remove residual chlorine and metal chlorides from the CDC samples. This procedure was carried out for 1 h and the materials were cooled under flowing argon. Pyrolysis and high-temperature chlorine treatment of the microporous reference samples was performed under similar conditions as for the CDC aerogels; pure SMP-10 was used as the polymeric precursor.

Characterization

Prior to all adsorption measurements the samples were degassed under vacuum for at least 5 h. SiC and CDC samples were heated up to 150 °C, and polycarbosilane aerogels were activated at 50 °C. Nitrogen (−196 °C) and carbon dioxide (0 °C) measurements were performed using an Autosorb 1C apparatus and the ASiQwin analysis software (Quantachrome Instruments, Boynton Beach, USA). Specific surface areas were calculated according to the Brunauer–Emmett–Teller (BET) equation in the range from 0.05–0.20p/p_0 in the case of aerogel materials and from 0.01–0.10p/p_0 for the microporous reference samples. Total pore volumes were calculated using the Gurvich rule at $p/p_0 = 0.99$. Pore size distributions were calculated from the nitrogen adsorption isotherms using the quenched solid density functional theory (QSDFT, nitrogen on carbon slit/cylindrical adsorption branch kernel) method. In the case of microporous CDC reference samples the QSDFT, nitrogen on carbon slit pores equilibrium branch kernel was used. Pore volumes < 1.0 nm were obtained by applying the non-local density functional theory (NLDFT, carbon dioxide on carbon) to the carbon dioxide physisorption isotherms.

Mercury intrusion porosimetry was performed using a PoreMaster-60 GT from Quantachrome Instruments (Boynton Beach, USA). The pore size distributions were calculated from the mercury intrusion data by applying the Washburn equation. A contact angle of 140° was used for the calculation as well as a surface tension of 480 ergs.

Thermal response of the samples was measured using the previously described optical calorimeter setup (InfraSorp Technology by Fraunhofer/Rubotherm).[26] Small amounts of sample (5–25 mg) were placed in the sample cell and purged with nitrogen until a constant sample temperature was observed. When the sample was at constant temperature, it was exposed to a flow of 70 sccm (25 °C, 1013 kPa) CO_2 using a mass flow controller. The thermal response function was fitted to the measured data using Origin 7.5 software.

Scanning Electron Microscopy (SEM) investigations were carried out with a DSM982 microscope (Zeiss, Germany) with an EDX analysis system using secondary electrons and back-scattered electrons detectors, respectively. Elemental analyses using Electron dispersive X-ray spectroscopy (EDX) were obtained as a mean value of three measurements at a magnification of 5000. Transmission electron microscopy investigations were performed using a Cs-corrected JEOL JEM-2010F microscope.

Results and discussion

PCS gels were obtained by cross-linking liquid allylhydridopolycarbosilane (SMP-10) with *p*-DVB in cyclohexane using the hydrosilylation catalyzed by a platinum complex (platinum–divinyltetramethyldisiloxane) according to a method recently reported by Sorarù and co-workers.[24] After drying under supercritical carbon dioxide, the white PCS aerogels were pyrolyzed to aerogel-structured SiC at the maximum temperature of either 700 °C or 1000 °C, and finally the silicon extraction was performed in an atmosphere of hot chlorine gas at the maximum pyrolysis temperature (Fig. 1).

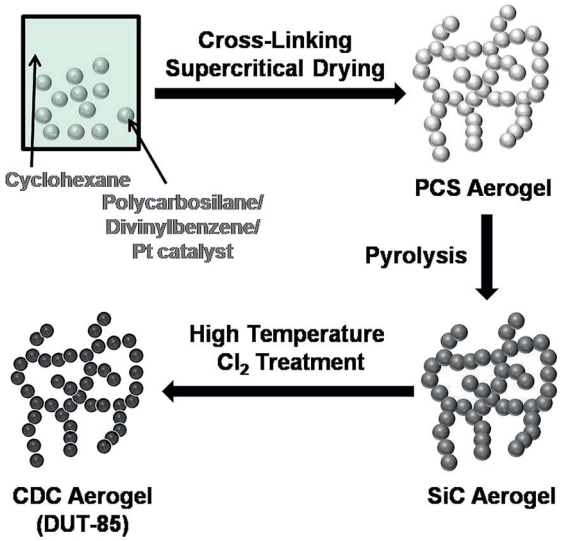

Fig. 1 Synthesis procedure of DUT-85.

During the conversion from polymer to carbide, linear volume shrinkage of 30 and 40% was observed at pyrolysis temperatures of 700 and 1000 °C, respectively (ESI, Fig. S1†). This difference is caused by different temperature-dependent crystallization states and inter-atomic distances within the silicon carbides at different synthesis temperatures.[15] Consequently, the decrease of the initial Brunauer–Emmett–Teller specific surface area (SSA) (Table 1) of the PCS aerogel (507 $m^2 g^{-1}$) after pyrolysis is more distinct for the SiC aerogel obtained at 1000 °C (307 $m^2 g^{-1}$) compared to the low temperature sample (463 $m^2 g^{-1}$). Their nitrogen physisorption isotherms (Fig. S2†) show typical appearance for aerogels including high uptake at $p/p_0 > 0.9$ due to adsorption in the aerogel macropore system. Accordingly, scanning electron microscopy (SEM) micrographs of the PCS and SiC aerogels (Fig. S3†) show the typical macroporous open cell foam morphology consisting of interconnected nanometer-sized primary particles. Due to the lower degree of volume shrinkage at a pyrolysis temperature of 700 °C, the particle size is larger and more distinct inter-particular and open porosity can be observed when compared with the SiC aerogel obtained at 1000 °C leading to the larger increase in the volume at the highest relative pressure in the nitrogen physisorption analyses (Fig. S2†). EDX measurements show that, in comparison with other polymer-derived CDC precursors,[19] the carbon/silicon molar ratio of the SiC aerogels is higher due to the use of a large amount of carbon containing *p*-DVB cross-linker which is necessary to obtain a stable and well-defined PCS aerogel (Table S1†). Since the high-temperature chlorination process is fully conformal, no macroscopic changes can be observed during the carbide-to-carbon transformation (Fig. S1†). The monolithic shape of the aerogels can be kept intact over the entire synthesis pathway, a feature that is beneficial in many applications.

DUT-85 materials show the typical aerogel-type pore system. A more distinct open porosity can be observed at lower synthesis temperatures according to the SiC aerogel precursors (Fig. 2). Transmission electron microscopy images (Fig. 3) show the highly amorphous carbon microstructure consisting of mainly disordered sp^2 carbon fringes. DUT-85 materials do not show distinctive graphitic stacking as it is typical for polymer-based CDCs within the investigated range of synthesis temperatures.

Nitrogen physisorption at −196 °C (Fig. 4) isotherms show that DUT-85 materials exhibit the typical aerogel-type shape with large gas uptake at relative pressures $p/p_0 > 0.9$ due to adsorption in large meso- and macropores indicating the presence of very high pore volumes. The higher amount of adsorbed nitrogen in the low-pressure region (Fig. 4, inset) compared to the SiC aerogels is associated with the filling of narrow micropores present in DUT-85 after silicon extraction, which significantly increase the specific surface areas (SSAs) to 2122 $m^2 g^{-1}$ and 1675 $m^2 g^{-1}$ for DUT-85 prepared at 700 °C and 1000 °C, respectively (Table 1). Despite the similar micropore volumes, the SSAs considerably depend on the applied synthesis temperature indicating its strong influence on the microstructure.

The temperature-dependent structure of DUT-85 was additionally characterized by carbon dioxide physisorption at 0 °C and atmospheric pressure (Fig. 5), which is a useful

Table 1 Porosity data summary of the PCS aerogel as well as the SiC and CDC aerogels (DUT-85) at different synthesis temperatures

Sample	SSA[a] [$m^2\ g^{-1}$]	$V_{pore,\ <2\ nm}$[b] [$cm^3\ g^{-1}$]	$V_{pore,\ <1.0\ nm}$[c] [$cm^3\ g^{-1}$]	$V_{pore,\ meso+macro}$[d] [$cm^3\ g^{-1}$]
PCS aerogel	507	0.03	Not measured	Not measured
SiC aerogel 700 °C	463	0.06	0.07	4.56
SiC aerogel 1000 °C	307	0.03	0.04	3.26
CDC aerogel 700 °C	2122	0.50	0.27	8.43
CDC aerogel 1000 °C	1675	0.51	0.30	5.01

[a] Specific surface areas calculated from nitrogen physisorption using the BET equation (0.05–0.20p/p_0). [b] Micropore volume calculated from QSDFT cumulative pore volumes from nitrogen physisorption at a diameter of 2 nm. [c] NLDFT cumulative pore volumes from carbon dioxide physisorption at a diameter of 1.0 nm. [d] Meso- and macropore volumes calculated by mercury intrusion porosimetry.

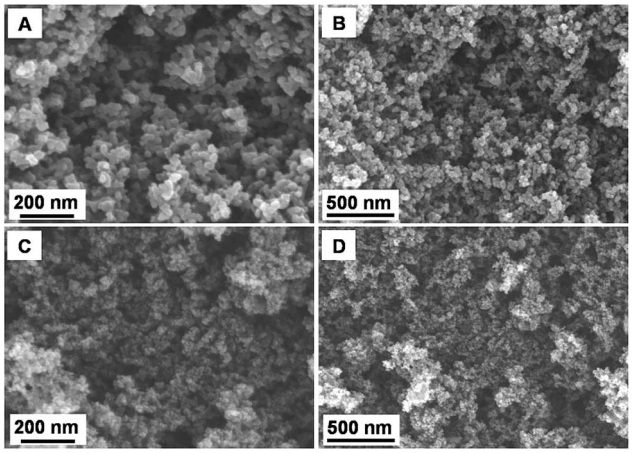

Fig. 2 Scanning electron microscopy images of DUT-85 prepared at (A and B) 700 °C and (C and D) 1000 °C.

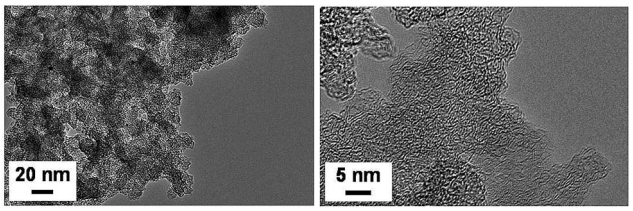

Fig. 3 Transmission electron microscopy images of DUT-85 prepared at 700 °C.

molecule for the analysis of narrow micropores due to its ability to access pores smaller than those that can be accessed using nitrogen adsorption at −196 °C. CO_2 at 0 °C diffuses more rapidly into the narrow micropores and pore filling occurs at higher relative pressures than for nitrogen. For the adsorption of large quantities of carbon dioxide, pores with diameters below 1.0 nm are largely required. Independent of the elevated temperature, the creation of micropores during the chlorine treatment significantly increases the amount of adsorbed CO_2 in DUT-85 as compared to the SiC aerogels. However, while silicon was quantitatively removed, the micropore structure of DUT-85 became very sensitive to the temperature of pyrolysis and chlorine treatment.

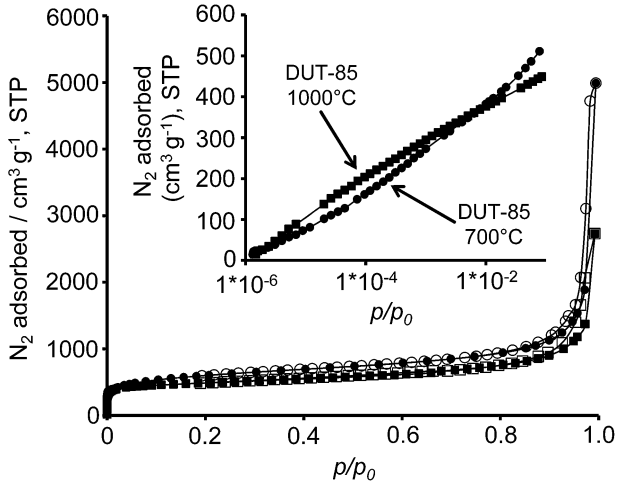

Fig. 4 Linear and semi-logarithmically (inset, low pressure region) plotted nitrogen physisorption isotherms (−196 °C) of DUT-85 prepared at 700 °C (circles) and 1000 °C (squares).

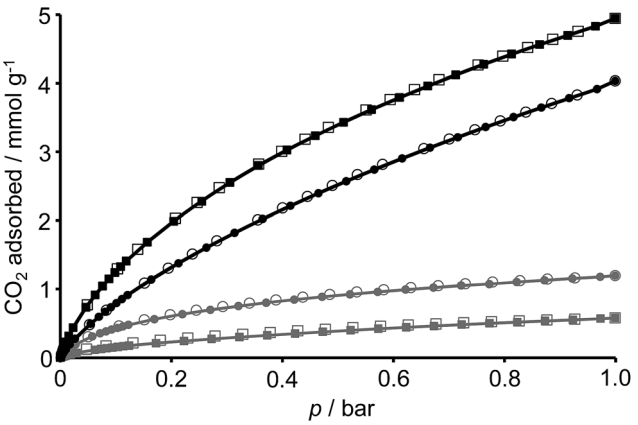

Fig. 5 Carbon dioxide (0 °C) adsorption/desorption (filled symbols/empty symbols) isotherms of DUT-85 (black) and the SiC precursor aerogels (grey) prepared at 1000 °C/700 °C (squares/circles).

The characterization of the micropore structure by the density functional theory (DFT) analysis of combined carbon dioxide and low-pressure nitrogen physisorption (Fig. 6, S4 and S5†) shows the presence of a higher volume of pores < 1.0 nm in

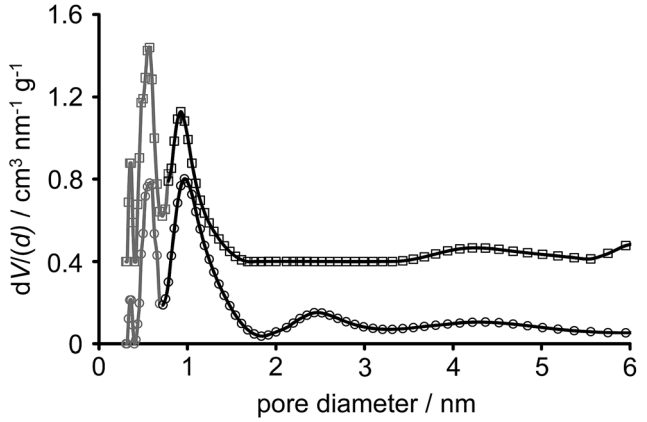

Fig. 6 Differential pore volumes of DUT-85 (700 °C) (circles) and DUT-85 (1000 °C) (squares) obtained from combined DFT analysis of carbon dioxide (grey) and nitrogen (black) physisorption isotherms. The differential pore volume of DUT-85 1000 °C is vertically offset by 0.4 $cm^3\ nm^{-1}\ g^{-1}$.

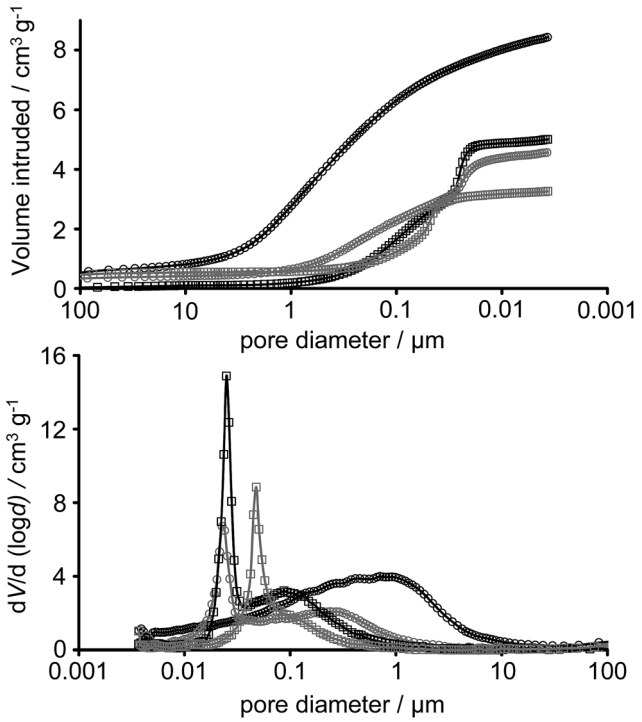

Fig. 7 Mercury intrusion curves (top) and corresponding pore size distributions (bottom) of DUT-85 (black) and the SiC precursor aerogels (grey) prepared at 1000 °C/700 °C (squares/circles).

DUT-85 1000 °C (Table 1, Fig. S6†) being responsible for the higher uptake of carbon dioxide at ambient pressure. The larger inter-atomic distances between the carbon atoms in the less crystalline SiC aerogel 700 °C and the preferred formation of amorphous carbon instead of graphitic nanodomains cause the formation of larger micropores and higher specific surface areas in the finally obtained DUT-85 compared to the synthesis at 1000 °C where a higher volume of narrow micropores is obtained. Additionally, a small portion of mesopores is present independent of the elevated synthesis temperature, as is typical for hierarchical CDCs obtained by catalyzed cross-linking of polycarbosilanes.[19]

The large uptake at high relative pressures in the nitrogen physisorption isotherms as well as the increase in pore volume from the silicon carbide precursors to the CDC indicates the presence of the aerogel-type macropore system. Quantitative analysis of the large-pore systems present in the aerogels (volume, size distribution) is not possible from the nitrogen physisorption data. Therefore, mercury intrusion porosimetry measurements were performed to determine the porosity within the aerogel monoliths. Despite the fact that the mercury porosimetry data indicate the possibility of some (reversible) material compression (see intrusion/extrusion data in Fig. S7†), the mercury intrusion curves (Fig. 7) show the same trend as the nitrogen physisorption measurements. A larger volume of liquid is intruded into the carbide-derived carbons compared to the silicon carbide precursors. The highly open and well-accessible pore structure present in DUT-85 causes meso-/macropore volumes as high as 8.43 $cm^3\ g^{-1}$ and 5.01 $cm^3\ g^{-1}$ for the CDC materials synthesized at 700 and 1000 °C, respectively (Table 1). If the simultaneous presence of the micropores, which are not detected in these measurements, is taken into consideration, DUT-85 offers total pore volumes close to 9 $cm^3\ g^{-1}$. The lower pore volumes of the carbide and carbon aerogels prepared at a higher temperature are likely related to the higher degree of volume shrinkage during the conversion from PCS aerogel to carbide leading to rather dense materials as has already been indicated by the SEM studies (Fig. 2). With the exception of DUT-85 700 °C, all aerogels show the presence of broadly distributed macropores in the range of 0.5–1 μm and a narrow maximum centered at 0.025–0.05 μm. The latter is related to mercury intrusion in the empty spaces between two agglomerated nanoparticles being in direct contact while the larger pores are formed by the macroporous open cell foam structure built up by the nanoparticle chains. The monomodal distribution of pores in DUT-85 700 °C as well as the distinct intrusion of mercury at a larger pore diameter (lower pressure) indicates some structural change of this material, such as the collapse of the nanoparticle chains, during mercury intrusion and therefore a reliable pore size distribution cannot be determined for this sample.

The adsorption properties of hierarchical DUT-85 were compared with purely microporous CDC reference materials prepared by pyrolysis of polycarbosilane SMP-10 at 700 (Micro-CDC 700 °C) or 1000 °C (Micro-CDC 1000 °C) followed by chlorine treatment at equal temperature. Both samples show type I nitrogen physisorption isotherms (−196 °C), according to the IUPAC classification as they are exclusively microporous (Fig. S8†). Compared to hierarchical DUT-85, the microporous CDCs show slightly higher specific surface areas of 2298 $m^2\ g^{-1}$ (700 °C) and 2117 $m^2\ g^{-1}$ (1000 °C) due to their larger micropore volumes (Table S2†). The latter are a result of the higher silicon/carbon ratio in the carbide precursors of microporous CDC obtained by pyrolysis of pure SMP-10 in the absence of any carbonaceous cross-linker. As for DUT-85, the presence of narrow micropores in the reference materials strongly depends

on the elevated synthesis temperature. The uptake of nitrogen reaches saturation at a lower relative pressure in the high-temperature sample due to the higher volume of small ultra-micropores leading to higher CO_2 adsorption capacity (Fig. S9†) compared to the material prepared at 700 °C. Both microporous samples offer higher CO_2 uptakes compared to the DUT-85 analogues obtained at the same temperature and seem to be more attractive candidates for the removal of carbon dioxide by preferential adsorption on the first view. However, another important requirement to an effective adsorbent material is rapid adsorption kinetics, and the narrower the pores and the more compact the material, mass transfer restrictions are likely to occur.

Recently, thermal response measurements are presented as an efficient tool for the screening of materials properties such as specific surface area, adsorption capacity, and -kinetics.[26] In this method, the real-time resolved temperature change, which is caused by the heat of adsorption, is measured using an optical calorimeter. The adsorption of CO_2 at 25 °C and ambient pressure ($p/p_0 \sim 0.02$) was used to investigate the influence of the hierarchical pore structure present in DUT-85 on the adsorption kinetics in comparison with the microporous CDC reference materials. According to the measurements under equilibrium conditions at 0 °C, the specific thermal response peak areas of DUT-85 and the microporous reference prepared at 1000 °C are about 1.3 fold larger than those of the low temperature samples indicating their larger uptakes at 25 °C (Fig. 8).

Since the time-constant for the optical calorimeter is negligible, the temperature signal can be directly evaluated in terms of adsorption kinetics. Previously we proposed a thermal response function (eqn (1)) assuming that the adsorption process follows first order kinetics, the heat released is proportional to the amount of adsorbed gas, and the heat transfer is constant during time.[26]

$$\Delta T(t) = \Delta T_1[(1 - e^{-k_1 t}) - (1 - e^{-k_2 t})] \quad (1)$$

By fitting eqn (1) (ΔT: measured temperature change, ΔT_1: maximum adiabatic temperature, k_1: thermal rate constant, k_2: rate of heat transfer) to the measured thermal response curve, the thermal adsorption rate constant is obtained. The fit quality R^2 is above 0.998 for all samples except for Micro-CDC 1000 °C with R^2 of 0.988 (Fig. S10†). If the model sufficiently describes the measured data, integration of eqn (1) should give the same peak area obtained by numerical integration of the signal. This is the case for Micro-CDC 700 °C, DUT-85 700 °C and DUT 85 1000 °C where the peak areas (calculation from function *vs.* numerical integration) show deviations of only 5.0%, 1.4% and 4.4%, respectively. For the Micro-CDC 1000 °C sample a much larger deviation of 33% is calculated because the function does not sufficiently describe the long term equilibration behaviour of the measured data for this material containing the narrowest micropores and no transport pore arrangement. According to the earlier work of Reucroft and Rivin,[27] we modified the thermal response function by a second process describing the migration of molecules adsorbed in easily accessible larger pores to the stronger adsorption sites in the more narrow micropores. Consequently, an additional thermal response peak was introduced in eqn (1), giving eqn (2) (ΔT_2: maximum adiabatic temperature of the migration process, k_3: thermal rate constant of the migration, k_4: rate of heat transfer for the migration process).

$$\Delta T(t) = \Delta T_1[(1 - e^{-k_1 t}) - (1 - e^{-k_2 t})] + \Delta T_2[(1 - e^{-k_3 t}) - (1 - e^{-k_4 t})] \quad (2)$$

Using eqn (2) for fitting to the thermal response of the microporous reference sample prepared at 1000 °C gives good quality for the entire range of the data (Fig. S11†). The disappearance of the second peak for the DUT-85 1000 °C indicates enhanced kinetics in carbon dioxide adsorption due to superior accessibility of the micropores provided by the meso/macropore system. Moreover, the obtained overall adsorption rate constants k_1 show a direct correlation between the pore structure of the investigated materials and their adsorption kinetics. Independent of the synthesis temperature, strictly microporous CDCs show significantly slower adsorption constants ($k_1 = 1.04\ s^{-1}$ for synthesis at 1000 °C and $k_1 = 1.28\ s^{-1}$ for synthesis at 700 °C) compared to DUT-85 ($k_1 = 2.07\ s^{-1}$ for synthesis at 1000 °C and $k_1 = 3.83\ s^{-1}$ for synthesis at 700 °C, Fig. S12†). For both systems a faster adsorption can be observed in the samples prepared at the lower temperature indicating that the presence of larger micropores enhances the kinetics as well.

A comparison of CO_2 adsorption properties of the CDC materials presented here and NaKA zeolites reported by Akhtar and co-workers shows a higher CO_2 storage capacity for the zeolites due to their rather narrow micropores.[28] However, the crystalline solids do not reach saturation even after 15 min of CO_2 adsorption. In contrast, the CDC aerogels reach equilibrium temperature even after 30 s due to their advanced pore structure for rapid adsorption kinetics.

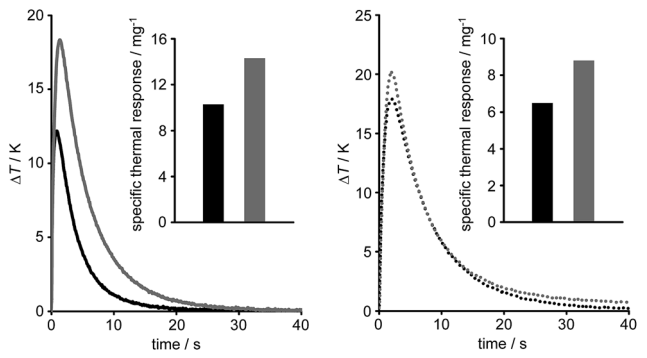

Fig. 8 Thermal response curves for carbon dioxide adsorption at 25 °C and corresponding integrated specific thermal response peak areas (insets) of DUT-85 (left, straight lines) and the microporous CDC reference materials (right, dotted lines) prepared at 1000 °C/700 °C (grey/black).

Conclusions

We have presented a novel pathway for the preparation of carbide-derived carbon aerogels (DUT-85) by platinum catalyzed hydrosilylation of polycarbosilanes followed by supercritical

drying, ceramic conversion and high-temperature chlorine treatment. DUT-85 materials exhibit specific surface areas larger than 2100 $m^2 g^{-1}$ and total pore volumes close to 9 $cm^3 g^{-1}$ due to the simultaneous presence of a large micropore volume and the aerogel type structure of agglomerated nanoparticles. The micropore structure is precisely controllable by the synthesis temperature and can be tuned for the adsorption of large capacities of carbon dioxide. Advanced adsorption kinetics are detectable in comparison with reference materials without transport pores, but comparable microstructure renders DUT-85 as a highly efficient adsorbent and promising component for any application where a combination of large capacities and efficient materials transport is required.

Acknowledgements

The authors gratefully acknowledge financial support by the German Research Foundation (DFG) for the project "Adsorption kinetics in hierarchical porous carbide-derived carbon materials".

Notes and references

1 V. Presser, M. Heon and Y. Gogotsi, *Adv. Funct. Mater.*, 2011, **21**, 810; Y. Gogotsi, A. Nikitin, H. Ye, W. Zhou, J. E. Fischer, B. Yi, H. C. Foley and M. W. Barsoum, *Nat. Mater.*, 2003, **2**, 591.

2 Y. Gogotsi, R. K. Dash, G. Yushin, T. Yildirim, G. Laudisio and J. E. Fischer, *J. Am. Chem. Soc.*, 2005, **127**, 16006; M. Sevilla, R. Foulston and R. Mokaya, *Energy Environ. Sci.*, 2010, **3**, 223; A. Silvestre-Albero, S. Rico-Francés, F. Rodriguez-Reinoso, A. M. Kern, M. Klumpp, B. J. M. Etzold and J. Silvestre-Albero, *Carbon*, 2013, **59**, 221.

3 J. J. Niu, V. Presser, C. J. Karwacki and Y. Gogotsi, *Mater. Express*, 2013, **1**, 259; L. Borchardt, F. Hasché, M. R. Lohe, M. Oschatz, F. Schmidt, E. Kockrick, C. Ziegler, T. Lescouet, A. Bachmatiuk, B. Büchner, D. Farrusseng, P. Strasser and S. Kaskel, *Carbon*, 2012, **50**, 1861.

4 G. Yushin, E. N. Hoffman, M. W. Barsoum, Y. Gogotsi, C. A. Howell, S. R. Sandeman, G. J. Phillips, A. W. Lloyd and S. V. Mikhalovsky, *Biomaterials*, 2006, **27**, 5755; V. Presser, S.-H. Yeon, C. Vakifahmetoglu, C. A. Howell, S. R. Sandeman, P. Colombo, S. Mikhalovsky and Y. Gogotsi, *Adv. Healthcare Mater.*, 2012, **1**, 796.

5 J. Chmiola, G. Yushin, Y. Gogotsi, C. Portet, P. Simon and P. L. Taberna, *Science*, 2006, **313**, 1760; J. Chmiola, C. Largeot, P. L. Taberna, P. Simon and Y. Gogotsi, *Angew. Chem., Int. Ed.*, 2008, **47**, 3392; C. R. Pérez, S. H. Yeon, J. Ségalini, V. Presser, P. L. Taberna, P. Simon and Y. Gogotsi, *Adv. Funct. Mater.*, 2013, **23**, 1081; D.-D. Zhou, H.-J. Liu, Y.-G. Wang, C.-X. Wang and Y.-Y. Xia, *J. Mater. Chem.*, 2012, **22**, 1937; S.-H. Yeon, K.-N. Jung, S. Yoon, K.-H. Shin and C.-S. Jin, *J. Phys. Chem. Solids*, 2013, **74**, 1045; J. Leis, M. Arulepp, A. Kuura, M. Lätt and E. Lust, *Carbon*, 2006, **44**, 2122.

6 R. K. Dash, A. Nikitin and Y. Gogotsi, *Microporous Mesoporous Mater.*, 2004, **72**, 203; R. K. Dash, G. Yushin and Y. Gogotsi, *Microporous Mesoporous Mater.*, 2005, **86**, 50.

7 E. N. Hoffman, G. Yushin, T. El-Raghy, Y. Gogotsi and M. W. Barsoum, *Microporous Mesoporous Mater.*, 2008, **112**, 526; J.-S. Bae, T. X. Nguyen and S. K. Bhatia, *J. Phys. Chem. C*, 2010, **114**, 1046.

8 J. Chmiola, C. Largeot, P. L. Taberna, P. Simon and Y. Gogotsi, *Science*, 2010, **328**, 480.

9 M. Kormann and N. Popovska, *Microporous Mesoporous Mater.*, 2010, **130**, 167; M. Kormann, H. Gerhard and N. Popovska, *Carbon*, 2009, **47**, 242.

10 S. H. Yeon, I. Knoke, Y. Gogotsi and J. E. Fischer, *Microporous Mesoporous Mater.*, 2010, **131**, 423; J. Wang, M. Oschatz, T. Biemelt, L. Borchardt, I. Senkovska, M. R. Lohe and S. Kaskel, *J. Mater. Chem.*, 2012, **22**, 23893.

11 S. H. Yeon, P. Reddington, Y. Gogotsi, J. E. Fischer, C. Vakifahmetoglu and P. Colombo, *Carbon*, 2010, **48**, 201.

12 H. Nishihara and T. Kyotani, *Adv. Mater.*, 2012, **24**, 4473; A.-H. Lu and F. Schüth, *Adv. Mater.*, 2006, **18**, 1793; L. Borchardt, C. Hoffmann, M. Oschatz, L. Mammitzsch, U. Petasch, M. Herrmann and S. Kaskel, *Chem. Soc. Rev.*, 2012, **41**, 5053.

13 L. Borchardt, M. Oschatz, M. Lohe, V. Presser, Y. Gogotsi and S. Kaskel, *Carbon*, 2012, **50**, 3987.

14 M. Oschatz, E. Kockrick, M. Rose, L. Borchardt, N. Klein, I. Senkovska, T. Freudenberg, Y. Korenblit, G. Yushin and S. Kaskel, *Carbon*, 2010, **48**, 3987; M. Oschatz, L. Borchardt, S. Rico-Francés, F. Rodríguez-Reinoso, S. Kaskel and J. Silvestre-Albero, *Langmuir*, 2013, **29**, 8133.

15 M. Oschatz, L. Borchardt, K. Pinkert, S. Thieme, M. R. Lohe, C. Hoffmann, M. Benusch, F. M. Wisser, C. Ziegler, L. Giebeler, M. H. Rümmeli, J. Eckert, A. Eychmüller and S. Kaskel, *Adv. Energy Mater.*, 2014, **4**, 1300645.

16 M. Rose, Y. Korenblit, E. Kockrick, L. Borchardt, M. Oschatz, S. Kaskel and G. Yushin, *Small*, 2011, **7**, 1108.

17 J. T. Lee, Y. Zhao, S. Thieme, H. Kim, M. Oschatz, L. Borchardt, A. Magasinski, W. I. Cho, S. Kaskel and G. Yushin, *Adv. Mater.*, 2013, **25**, 4573.

18 Y. Wang, X. Wang, M. Antonietti and Y. Zhang, *ChemSusChem*, 2010, **3**, 435; L. Chuenchom, R. Kraehnert and B. M. Smarsly, *Soft Matter*, 2012, **8**, 10801.

19 M. Oschatz, L. Borchardt, M. Thommes, K. A. Cychosz, I. Senkovska, N. Klein, R. Frind, M. Leistner, V. Presser, Y. Gogotsi and S. Kaskel, *Angew. Chem., Int. Ed.*, 2012, **51**, 7577; M. Oschatz, L. Borchardt, I. Senkovska, N. Klein, M. Leistner and S. Kaskel, *Carbon*, 2013, **56**, 139.

20 M. Oschatz, S. Boukhalfa, W. Nickel, J. T Lee, S. Klosz, L. Borchardt, A. Eychmüller, G. Yushin and S. Kaskel, *J. Mater. Chem. A*, 2014, **2**, 5131.

21 D. N. Futaba, K. Hata, T. Yamada, T. Hiraoka, Y. Hayamizu, Y. Kakudate, O. Tanaike, H. Hatori, M. Yumura and S. Iijima, *Nat. Mater.*, 2006, **5**, 987.

22 J. Biener, M. Stadermann, M. Suss, M. A. Worsley, M. M. Biener, K. A. Rose and T. F. Baumann, *Energy Environ. Sci.*, 2011, **4**, 656; R. J. White, N. Brun,

V. L. Budarin, J. H. Clark and M.-M. Titirici, *ChemSusChem*, 2014, **3**, 670.

23 S. Osswald, C. Portet, Y. Gogotsi, G. Laudisio, J. P. Singer, J. E. Fischer, V. V. Sokolov, J. A. Kukushkina and A. E. Kravchik, *J. Solid State Chem.*, 2009, **182**, 1733.

24 G. D. Sorarù, F. Dalcanale, R. Campostrini, A. Gaston, Y. Blum, S. Carturan and P. R. Aravind, *J. Mater. Chem.*, 2012, **22**, 7676.

25 J. Wang, I. Senkovska, M. Oschatz, M. R. Lohe, L. Borchardt, A. Heerwig, Q. Liu and S. Kaskel, *ACS Appl. Mater. Interfaces*, 2013, **5**, 3160; M. Sevilla, C. Falco, M.-M. Titirici and A. B. Fuertes, *RSC Adv.*, 2012, **2**, 12792; L. Zhao, Z. Bacsik, N. Hedin, W. Wei, Y. Sun, M. Antonietti and M.-M. Titirici, *ChemSusChem*, 2010, **3**, 840; J. Wang, A. Heerwig, M. R. Lohe, M. Oschatz, L. Borchardt and S. Kaskel, *J. Mater. Chem.*, 2012, **22**, 13911; R. Dawson, E. Stöckel, J. R. Holst, D. J. Adams and A. I. Cooper, *Energy Environ. Sci.*, 2011, **4**, 4239; J.-R. Li, Y. Ma, M. C. McCarthy, J. Sculley, J. Yu, H.-K. Jeong, P. B. Balbuena and H.-C. Zhou, *Coord. Chem. Rev.*, 2011, **255**, 1791.

26 M. Leistner, W. Grählert and S. Kaskel, *Chem. Ing. Tech.*, 2013, **85**, 747.

27 P. J. Reucroft and D. Rivin, *Thermochim. Acta*, 1999, **328**, 19.

28 F. Akhtar, Q. Liu, N. Hedin and L. Bergström, *Energy Environ. Sci.*, 2012, **5**, 7664.